Check for updates

Direct upcycling of degraded NCM *via* low-temperature surface engineering for high performance lithium-ion batteries†

Yu Wang and Chris Yuan [iD] *

Upcycling degraded low-Ni cathode materials into Ni-rich alternatives offers significant economic and environmental benefits for lithium-ion battery production. However, the stability and safety of the upcycled materials remain challenging due to their aggressive composition. This study reports an innovative two-step upcycling method that integrates a coating process with a low-temperature annealing process, thereby successfully upcycling degraded NCM622 with a $LiAlO_2$ coating layer. Through comprehensive characterization, the recovery of crystal structure and uniform $LiAlO_2$ coating on the particle surface are confirmed by XRD and XPS results. As a result of structural recovery and surface engineering, upcycled NCM622 demonstrates an initial capacity comparable to that of NCM811 at 195.3 mA h g^{-1} at 1 C rate, with 86.8% capacity retention after 100 cycles at a cut-off voltage of 4.6 V. Moreover, it exhibits excellent rate capability, delivering 141.9 mA h g^{-1} at 5 C. Beyond enhancing electrochemical performance, this method significantly improves the thermal stability of degraded NCM622, with the upcycled material showing less than 0.1% weight loss at 400 °C. The findings highlight the potential of upcycled cathode materials with the $LiAlO_2$ coating to meet the high-performance and sustainability requirements of modern lithium-ion batteries, contributing to the circular economy of lithium-ion batteries in the future.

Broader context

The transition to sustainable energy storage systems is critical for achieving global climate goals, with lithium-ion batteries playing a central role in electrifying transportation. However, the rapid growth of electric vehicles raises concerns about resource depletion and waste management of critical battery materials. While traditional recycling focuses primarily on material recovery, there is an urgent need for more sustainable approaches that can both recover and enhance the performance of degraded materials. Our innovative upcycling strategy demonstrates that end-of-life cathode materials can be transformed into high-performance components while reducing the environmental footprint of battery production. By combining coating and low-temperature annealing processes, this method not only recovers but significantly enhances the electrochemical performance and thermal stability of degraded materials, addressing both sustainability and safety challenges. The successful implementation of such upcycling approaches could dramatically reduce the need for primary raw material extraction while providing high-quality materials for next-generation batteries. This work establishes a new pathway toward circular material flows in the battery industry, contributing to both resource conservation and sustainable manufacturing practices.

Introduction

The rapid adoption of electric vehicles has driven unprecedented growth in lithium-ion battery (LIB) production, with global battery demand expected to reach 2600 GW h by 2030.[1] However, lithium-ion batteries of electric vehicles reach their end-of-life with less than 70% of their initial capacity after 8–10 years of service.[2] This relatively short lifespan has led to a substantial accumulation of spent LIBs, while the current global recycling rate of spent LIBs remains below 5%, presenting critical challenges in resource economics and environmental sustainability.[3] In a lithium-ion battery, cathode materials constitute the most valuable component for recycling, accounting for approximately 40% of the total battery cost[4] and containing a substantial amount of high-value transition metals such as Ni, Co, and Mn. To address these challenges, direct recycling methods have been proposed to recover the electrochemical performance of degraded cathode materials to their original states. Despite these efforts, the recycled cathode materials are outdated and often fail to meet the current performance standards of lithium-ion batteries for electric vehicles. For instance, NCM111, commonly used a

Department of Mechanical and Aerospace Engineering, Case Western Reserve University, 10900 Euclid Ave, Cleveland, Ohio 44016, USA.
E-mail: chris.yuan@case.edu

decade ago, delivers an energy density of 180 W h kg^{-1}, whereas contemporary NCM811 achieves over 280 W h kg^{-1}.[5] This performance gap not only demonstrates a critical limitation in conventional direct recycling methods but also necessitates the development of effective upcycling strategies to enhance the electrochemical performance of degraded cathode materials for sustainable battery manufacturing.

To achieve the upcycling of the degraded cathode materials, advanced technologies can be integrated into the direct recycling methods. Recent studies have explored various direct upcycling routes, including composition engineering, element doping, and structure reconstruction.[6] Composition engineering enhances the electrochemical performance of the degraded NCM materials by transforming low-Ni NCM to Ni-rich variants through high-temperature sintering with Ni salt. Kim et al. demonstrated this approach using reciprocal ternary molten salts to transform degraded NCM111 to NCM622, achieving a capacity of 180 mA h g^{-1} at 0.1 C with a capacity retention of 87.5% after 300 cycles.[7] Building on this concept, Ma et al. demonstrated an efficient upcycling method to transform spent polycrystalline LiNi$_{1/3}$Co$_{1/3}$Mn$_{1/3}$O$_2$ (NCM111) cathodes into high-performance single-crystal LiNi$_{0.6}$Co$_{0.2}$Mn$_{0.2}$O$_2$ (NCM622) by utilizing the rapid diffusion of nickel ions through NiO dissolution in molten Li$_2$CO$_3$, resulting in cathode materials with high phase purity and electrochemical performance comparable to commercial NCM622.[8] Another promising approach involves element doping methods, which involve lattice modification through ion substitution, enhance electrochemical performance by improving structural stability, Li$^+$ diffusion, and electronic conductivity. For example, Xing et al. reported an Al-doping method to upcycle degraded NCM523, achieving a capacity of 158.6 mA h g^{-1} at 0.1 C and 89.6% capacity retention at 1 C after 200 cycles.[9] Similarly, Ji et al. proposed a closed-loop upcycling strategy that repurposes waste current collector debris (Cu/Al) as dopants in a ternary eutectic molten salt system to transform highly degraded polycrystalline LiNi$_{0.83}$Co$_{0.12}$Mn$_{0.05}$O$_2$ into high-voltage cathode materials with superior electrochemical performance.[10] In addition to these methods, recent advances have also explored transitioning from degraded polycrystalline cathode materials to single-crystal variants, offering improved structural stability and more uniform volumetric change during cycling. Liu et al. demonstrated this by transforming degraded polycrystalline NCM622 to single-crystal NCM622, achieving a capacity of 171.9 mA h g^{-1} at 0.1 C and a capacity retention of 83.3% at 1 C after 200 cycles.[11] Further advancing this strategy, Shen et al. developed an innovative surface reconstruction strategy to effectively upcycle highly degraded polycrystalline NCM523 cathodes into single-crystal structures, employing a two-step approach where organic lithium salt (Li$_2$DHBN) transforms the surface rock salt phase into a layered structure, creating Li$^+$ diffusion channels that significantly reduce the energy barrier for lithium replenishment.[12] Despite these achievements, significant challenges still persist. Element doping and composition engineering methods are cost-intensive and energy-consuming, requiring substantial amounts of high-value metal salts and demanding high

sintering temperatures. Additionally, compositional inhomogeneity hinders large-scale application of these technologies. For structure reconstruction methods, the upcycled single-crystal cathode materials exhibit lower capacity than their polycrystalline counterparts.[13] In light of these limitations, it is imperative to develop more efficient and economically viable approaches for upcycling of degraded cathode materials.

Surface modification through advanced coating methods could be a promising alternative to address these challenges. Among various coating materials, LiAlO$_2$ stands out due to its superior performance of Li-ion conductivity.[14,15] The unique layered structure of LiAlO$_2$, similar to that of NCM, enables efficient lithium-ion diffusion pathways.[16] In this paper, an integration of advanced LiAlO$_2$ coating with direct recycling methods is achieved for the first time to enhance the electrochemical performance of the degraded NCM materials. Unlike element doping and composition engineering, surface modification can be achieved at lower sintering temperatures. Moreover, the coating process, which modifies only the particle surface, allows for superior uniformity compared to element doping and composition engineering approaches. The LiAlO$_2$ layer enhances the overall reaction kinetics of NCM materials while suppressing interfacial side reactions, thereby increasing capacity and enabling stable cycling at higher cut-off voltages.[17–20] As a result of these improvements, the rate capability of NCM materials is significantly improved, attributed to the high lithium-ion conductivity of the LiAlO$_2$ coating layer. Notably, the overall electrochemical performance of the upcycled NCM622 is comparable to that of the Ni-rich variants such as NCM811. In addition to the electrochemical enhancement, the LiAlO$_2$ coating enhances both thermal stability and safety of the upcycled NCM materials. From a practical perspective, the surface modification process remains cost-effective due to the low cost of precursor materials.

In this study, we report an upcycling method to enhance the electrochemical performance of degraded NCM622 cathode materials. The upcycling process simultaneously accomplishes two key objectives: fully recovering both lithium loss and structural degradation while converting the coating precursor to a LiAlO$_2$ layer. By addressing these aspects, this dual-function approach operates at a low temperature with a short sintering time, significantly enhancing the electrochemical performance of the degraded NCM622 while minimizing energy consumption and cost. Through the efficient integration of processes, the proposed upcycling method represents a novel approach to revitalizing the degraded cathode active materials, effectively addressing the growing demand for high-performance battery components while advancing the sustainable development goals of the lithium-ion battery industry.

Experimental section

Material preparation

Pristine NCM (P-NCM) was purchased from MTI. To prepare the degraded NCM (D-NCM), as-received P-NCM was

immersed in a redox solution under continuous stirring to achieve the delithiation process. The solution was made by dissolving 3.5 g potassium persulfate ($K_2S_2O_8$, Sigma Aldrich) in 400 mL distilled water, with continuous stirring at 50 °C until complete dissolution. 10 g pristine NCM622 was then dispersed into the solution and subjected to magnetic stirring at 60 °C for 12 hours. Then, the solution was filtered, and the obtained black powder was washed 3 times with distilled water. The D-NCM was subsequently dried in a vacuum oven at 120 °C for 2 hours. The final lithium leaching rate of the D-NCM was approximately 15%.

Direct upcycling of cathode materials

To prepare the coating solution, 0.35 g $Al(NO_3)_3$ was added and stirred in the 25 mL distilled water until fully dissolved. Subsequently, 3 g D-NCM was dispersed into the solution and the solution was magnetically stirred at 50 °C for 10 min. The temperature of the solution was then increased to 90 °C, and 15 mL (30 wt%) ammonium hydroxide was gradually added to the solution. The solution was continuously stirred magnetically for 1 h. Then, the solution was filtered, and the black powder was washed 3 times with distilled water. An excess of 5% LiOH (0.15 g) was added to the dried powder, and the mixture was then sintered in a furnace at 600 °C for 4 h. The upcycled NCM622 (Up-NCM-2) with 2 wt% $LiAlO_2$ coating layer was finally obtained by grinding the sintered powder using a mortar and pestle. The prepared cathode materials are labeled Up-NCM-1 (1 wt% $LiAlO_2$), Up-NCM-2 (2 wt% $LiAlO_2$), and Up-NCM-3 (3 wt% $LiAlO_2$).

Material characterization

The chemical compositions of D-NCM, P-NCM, and Up-NCM were measured by ICP-OES (PerkinElmer Optima 3000DV). The crystal structures of all samples were examined by XRD using a Rigaku SmartLab (Cu Kα radiation). SEM/EDS was carried out to observe the morphology of samples and investigate the element distribution on the particle surface using a ThermoFisher Apreo2. TEM was conducted to observe the $LiAlO_2$ layer on the Up-NCM particle surface, employing a FEI Tecnai G2 Spirit. XPS was conducted to study the oxidation states of elements on the surface of all samples using a PHI Versaprobe. TGA was carried out to measure the weight loss at high temperature using a TGA500.

Electrochemical characterization

D-NCM, P-NCM and Up-NCM were used as cathode active materials for cell assembly. The cathode active materials were mixed with polyvinylidene difluoride (PVDF) and Super P65 carbon black in N-methyl-2-pyrrolidone (NMP) with a mass ratio of 8 : 1 : 1 to prepare electrode slurries. The slurries were then uniformly spread on aluminum foil using a doctor blade and dried in a vacuum at 120 °C for 10 h. The electrodes were subsequently cut to disc-size and compressed using a double-roller calendering machine. The areal mass loading of the electrodes was approximately 3 mg cm^{-2}. Coin cells were assembled using these electrodes, with a Li metal disc
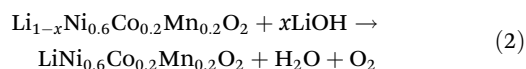
(1.1 mm thickness) as the counter electrode, 1.0 M LiPF$_6$ in EC/EMC = 3 : 7 as the electrolyte, and a Celgard 2500 monolayer membrane as the separator. Galvanostatic charge/discharge tests were conducted using a Neware battery testing system over a potential range of 2.7–4.6 V at various rates for 100 cycles, following initial 3 formation cycles at C/10. For performance evaluation, cycling tests were conducted in constant current-constant voltage (CCCV) protocol, while rate capability assessments were performed using constant current (CC) mode. Cyclic voltammetry (CV) tests were performed using a Versastat 3F at a scanning rate of 0.1 mV s^{-1} within the voltage range of 2.7–4.6 V. Electrochemical Impedance Spectroscopy (EIS) measurements were carried out using a Versastat 3F, applying an amplitude voltage of 5 mV over a frequency range from 1 Hz to 100 000 Hz. All the electrochemical tests were conducted in a temperature-controlled environment at 25 °C.

Results

To restore and improve the electrochemical performance and safety of D-NCM, a novel two-step upcycling method is proposed in this study. The upcycling method for D-NCM is illustrated in Fig. 1. In the initial phase, aluminum nitrate ($Al(NO_3)_3$) serves as the aluminum source for the coating, while an ammonia solution acts as the precipitant, facilitating the deposition of an ultrathin $Al(OH)_3$ layer on the surface of D-NCM particles. Following the deposition, the obtained NCM is then thoroughly rinsed with distilled water to eliminate the remaining salts. The process can be described by the chemical reaction in the first step of the upcycling process as follows:

$$Al(NO_3)_3 + NH_3 \cdot H_2O \rightarrow Al(OH)_3 + NH_4NO_3 \qquad (1)$$
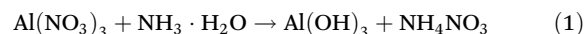
In the second stage of the upcycling process, lithium hydroxide (LiOH) is added to the NCM for two primary purposes: to recover the lithium loss in D-NCM and to transform the $Al(OH)_3$ coating into $LiAlO_2$. The temperature is set to 600 °C for the calcination step in the upcycling process. At this temperature, Li$^+$ from the molten LiOH migrates and reintegrates into the crystal lattice of D-NCM, compensating for the lithium loss. Simultaneously, the structural degradations, including anti-site mixing and distorted spinel structure, are also repaired by the high calcination temperature. During this process, the chemical reaction between $Al(OH)_3$ and LiOH occurs at this temperature, forming an ultrathin layer of $LiAlO_2$ on the regenerated particle surface. The chemical reactions occurring in this phase of the upcycling process are detailed as follows:

$$\begin{aligned} Li_{1-x}Ni_{0.6}Co_{0.2}Mn_{0.2}O_2 + xLiOH \rightarrow \\ LiNi_{0.6}Co_{0.2}Mn_{0.2}O_2 + H_2O + O_2 \end{aligned} \qquad (2)$$

$$Al(OH)_3 + LiOH \rightarrow LiAlO_2 + H_2O \qquad (3)$$

To investigate the composition recovery in the upcycling process, Inductively Coupled Plasma Optical Emission Spectrometry (ICP-OES) was employed to measure the compo-
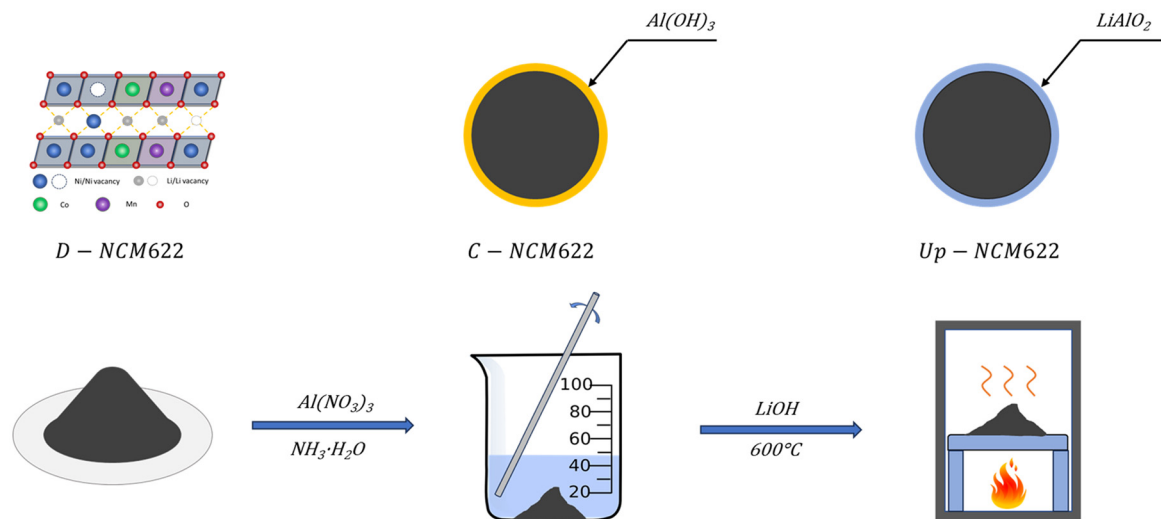
Fig. 1 Diagram of the two-step upcycling process.

sitions of Up-NCM, P-NCM, and D-NCM, with the results shown in Table S1.† It was observed that approximately 15% of lithium was extracted through the redox reaction with potassium persulfate in the delithiation process. Through the upcycling process, D-NCM was effectively recovered, exhibiting the same composition as the pristine material. The lithium content of D-NCM increased from 0.986 to 1.156, which is slightly higher than that of P-NCM. This high lithium content can be attributed to the intercalation of extra lithium into the D-NCM as a result of the high-temperature sintering.[21] Additionally, an ultrathin $LiAlO_2$ layer was successfully coated on the surface of NCM particles through the upcycling process.

While ICP-OES analysis confirmed the compositional recovery, further investigation of the structural evolution was necessary to fully characterize the material changes. During the upcycling process, the re-insertion of lithium and recovery of crystal structure occurred simultaneously with the conversion of the $Al(OH)_3$ coating layer to $LiAlO_2$ at high temperature. To investigate these crystal structure changes, X-ray powder diffraction (XRD) analyses were performed. The XRD patterns of D-NCM, P-NCM, and Up-NCM are presented in Fig. 2a. All samples displayed the typical diffraction pattern of the α-NaFeO$_2$ structure with $R\bar{3}m$ space group. This suggests that the delithiation process does not cause significant phase transition of D-NCM. However, as shown in Fig. 2c, the (003) peak in D-NCM shifts to a lower angle, corresponding to the expansion of the c-axis. Quantitative analysis reveals that the c-axis distance increases to 4.76 Å in D-NCM, compared to 4.73 Å in both P-NCM and Up-NCM, confirming the lattice expansion caused by lithium extraction. This is attributed to the increase of electrostatic repulsion between transition metal layers due to the Li$^+$ vacancy.[22] Along with this change, the increase of (108)/(110) peak distance, shown in Fig. 2d, is also observed in D-NCM, representing a decrease of the a-axis parameter. The explanation for this lies in the results of XPS, which shows

that the valence of Ni in NCM is a combination of Ni^{2+} and Ni^{3+}. Due to the extraction of lithium in D-NCM, Ni^{2+} was oxidized to Ni^{3+}, which has a smaller radius compared to Ni^{2+}, resulting in the contraction of a-axis.[23] Notably, D-NCM exhibited a significantly higher (003)/(104) intensity ratio of 1.34, compared to 1.16 for P-NCM and 1.15 for Up-NCM, quantitatively demonstrating the increased anti-site mixing levels in the degraded material. This increase is attributed to the lithium extraction in D-NCM during the chemical delithiation process, leading to Ni occupying unstable valence states (Ni^{3+} and Ni^{4+}). These states are prone to reducing to Ni^{2+} in the electrolyte environment.[24] Given the similar ionic radius of Ni^{2+} and Li$^+$, Ni^{2+} is likely to migrate from its original lattice position to that of Li$^+$, resulting in an increased intensity ratio of (003)/(104). Furthermore, the splitting of the (006)/(102) doublets is observed, a result of the distortion at the transition metal (TM) sites. This distortion leads to the migration of TM ions to Li$^+$ sites and initiates a phase transition from a layered structure to a spinel structure.[25] The (003) peak shifting back to its original position and the contraction of the (108)/(110) and (006)/(102) peak doublets are observed, confirming that both the lithium loss and the crystal structure of D-NCM are effectively recovered by the upcycling process. The (006)/(102) peak position shows that the Up-NCM has the same layered crystal structure as P-NCM and the crystal structure is not influenced by the upcycling process. Moreover, the (003)/(104) intensity ratio of Up-NCM is lower compared to P-NCM, which indicates that the anti-site mixing is further decreased by the upcycling process. In addition to the peaks of NCM, peaks of (101), (102), and (200) are observed within the range of 21° to 35° in the sample of Up-NCM, which is shown in Fig. 2b. These peaks are consistent with those of $LiAlO_2$ in the work of Lei *et al.*, which also proves the $LiAlO_2$ coating layer on the surface of Up-NCM.[26]

XPS analysis was employed to identify the coating layer composition by examining the oxidation states of Al, Ni, Co,
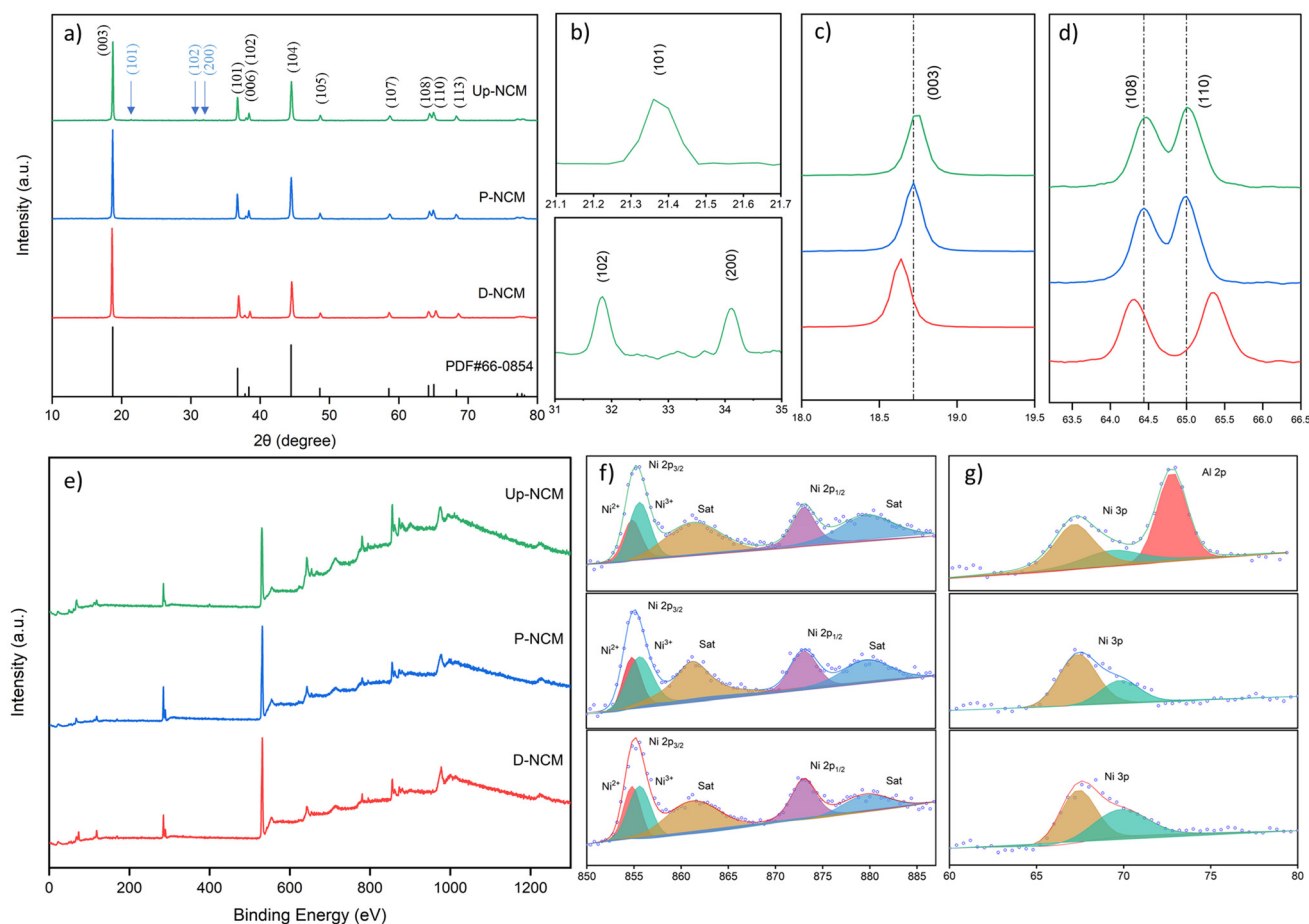
Fig. 2 XRD patterns and XPS spectra with fitting results of D-NCM, P-NCM, and Up-NCM, (a) full XRD patterns, (b) 31°–35°, (c) 18°–19.5°, (d) 63.5°–66.5°, (e) full XPS spectra, (f) Ni 2p, (g) Al 2p.

and Mn in all samples, with the complete elemental spectra shown in Fig. 2e. The Co 2p region exhibited characteristic peaks at 780.4 eV (Co 2p3/2) and 795.2 eV (Co 2p1/2), while the Mn 2p region showed consistent peaks at 641.2 eV (Mn 2p3/2) and 653.1 eV (Mn 2p1/2) across all samples. These values align with previous reports,[27] confirming that neither degradation nor upcycling affected the Co and Mn valence states. Fig. 2f presents the Ni 2p XPS spectra, revealing spin–orbit splitting with Ni 2p3/2 and Ni 2p1/2 peaks at 855.2 eV and 873.2 eV, respectively. These peaks indicate the presence of both Ni^{2+} and Ni^{3+} in the NCM particles. Notably, Up-NCM samples showed a reduced Ni^{2+} ratio compared to D-NCM and P-NCM, suggesting lower Li^{+}/Ni^{2+} anti-site mixing and a more balanced charge distribution on the Up-NCM surface. This result is consistent with the findings from the I003/I104 ratio analysis, which also demonstrated the lower anti-site mixing in Up-NCM compared to D-NCM, confirming the successful recovery of the crystal structure during the upcycling process. The Al 2p peak observed at 72.8 eV in Fig. 2g confirms the presence of Al on the Up-NCM surface. According to Negi et al.,[28] the Al 2p signal can be deconvoluted into two distinct peaks at 73.9 eV (Al_2O_3) and 72.8 eV ($LiAlO_2$). The observed Al 2p peak value in Up-NCM therefore confirms that the coating layer is $LiAlO_2$.

To explore the morphological change before and after the upcycling process, Scanning Electron Microscopy (SEM) analyses of D-NCM, P-NCM, and Up-NCM were conducted. Fig. 3a and b, and c reveal a uniform spherical morphology of all samples, with an average diameter of approximately 10 μm. These spherical particles consist of numerous primary particles. Notably, despite lithium loss and structural degradation, no morphological alterations were observed in D-NCM. Both D-NCM and P-NCM samples exhibit smooth surfaces, allowing for a clear view of individual primary particles. In contrast, Up-NCM is characterized by its rough surface, overlaid with a thin, nanoparticle coating layer, making it difficult to distinguish the primary particles on the surface. To evaluate the uniformity of the coating layer, Energy-dispersive X-ray Spectroscopy (EDS) mapping of Up-NCM was employed, enabling the examination of the elemental distribution (Al, Ni, Co, and Mn) across the particle surface. Fig. 3d illustrates that these elements are uniformly distributed, with the presence of Al confirming the continuous and uniform coating of the Al-based layer over the NCM microspheres. The following XRD and XPS results show that the composition of the Al-based coating layer is $LiAlO_2$. This coating serves dual functions: it acts as a thermal insulator and provides a protective layer, pre-
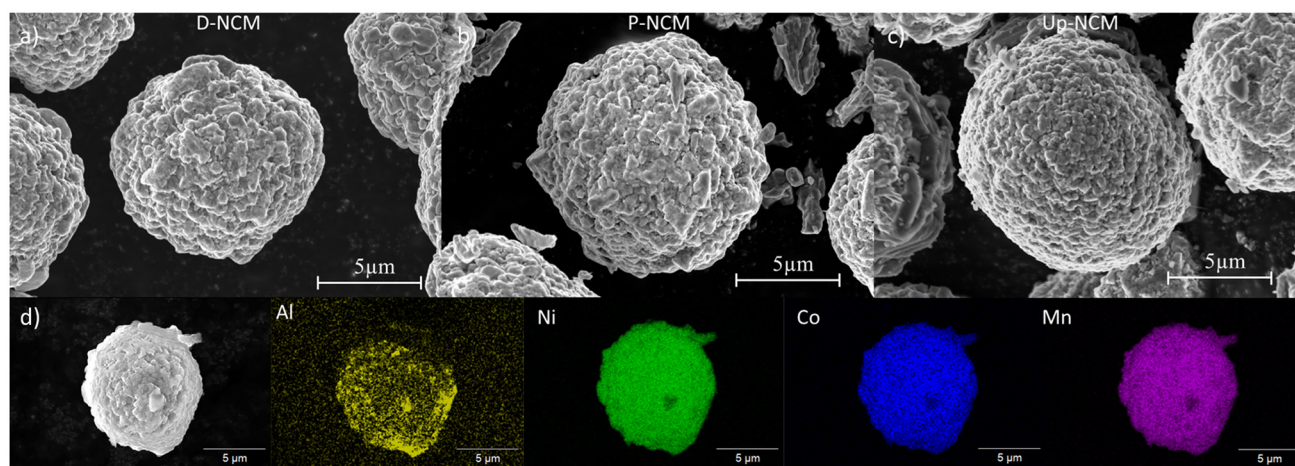
Fig. 3 SEM images of particles (a) D-NCM, (b) P-NCM, (c) Up-NCM, and (d) EDS mapping images of a Up-NCM particle.

venting direct contact between the NCM particles and the electrolyte. Therefore, the thermal and electrochemical stability of the NCM particles can be significantly enhanced by the $LiAlO_2$ coating layer. To further investigate the morphology, thickness, and uniformity of the $LiAlO_2$ coating layer, high-resolution TEM was performed, and the results are shown in Fig. S1.† The NCM particle and $LiAlO_2$ coating layer can be identified by the shape difference. In the TEM image, the dense material in the light grey area is the NCM particle, while the loose material in the outer dark layer is $LiAlO_2$. The TEM results, which are shown in Fig. S1,† confirmed that $LiAlO_2$ was homogeneously coated on the NCM particle surface by the two-step upcycling process. The distinct boundary between the NCM particle and the $LiAlO_2$ coating layer can also be observed. Additionally, the elemental mapping analysis across this interface further confirms this finding, with Fig. S2† clearly revealing the nickel, cobalt, and manganese distribution characteristic of the cathode material interior, while Fig. S3† shows the distribution of aluminum in the coating region with stoichiometric ratios consistent with $LiAlO_2$.

Through the upcycling process, the crystal structure of degraded NCM622 was fully recovered and a uniform $LiAlO_2$ coating layer was observed on the particle surface. To evaluate the cycling performance of D-NCM, P-NCM, and Up-NCM, the samples were subjected to cycling tests at a 1 C rate within a voltage range of 2.7–4.6 V. The results of all samples are shown in Fig. 4a. Due to the structural degradation, D-NCM shows a capacity of only 145.7 mA h g^{-1}, which nearly drops to 0 after 100 cycles. In comparison, P-NCM delivers an initial capacity of 187.8 mA h g^{-1} but experiences a sharp capacity reduction to 83.6 mA h g^{-1} after 100 cycles, corresponding to a capacity retention of 44.5%. This significant decline in the capacity of P-NCM is attributed to the higher anti-site mixing and Ni dissolution at high voltages.[29] Notably, the upcycled sample, Up-NCM-2, exhibits superior cycling performance, with an initial capacity of 195.3 mA h g^{-1} and an impressive capacity retention of 86.8% after 100 cycles. Similarly, Up-NCM-1 also displays enhanced cycling behavior, achieving a capacity retention of 71.7%. The improvement in cycling performance is attributed to the $LiAlO_2$ coating, which not only facilitates Li$^+$ diffusion and stabilizes the crystal structure under high voltage conditions but also serves to protect the NCM particles from direct contact with the electrolyte.[30] Although $LiAlO_2$ has high Li$^+$ conductivity, the electronic conductivity is poor.[31] Consequently, as the $LiAlO_2$ coating thickness increases, the low electronic conductivity of Up-NCM-3 becomes the limiting factor, resulting in high overall charge-transfer resistance. The higher charge transfer resistance initially limits the access to the full capacity in early cycles. The trade-off between protective properties and conductivity is well-documented in coating strategies for cathode materials. Despite the lower initial capacity, the cycling stability of Up-NCM-3 benefits from the $LiAlO_2$ coating layer, as evidenced by a capacity retention of 53.7%. In fact, despite its lower initial capacity, Up-NCM-3 demonstrates higher stability under high cut-off voltage conditions compared to the P-NCM. While the unprotected P-NCM undergoes progressive structural degradation, transition metal dissolution, and electrolyte decomposition at the particle surface, the thicker $LiAlO_2$ coating on Up-NCM-3 provides enhanced protection against these degradation mechanisms. When comparing the Up-NCM-2 with reported NCM811 materials, the upcycling method demonstrates superior cycling stability. Under the voltage range of 2.7–4.3 V, NCM811 delivers an initial capacity of approximately 180 mA h g^{-1} but experiences a capacity loss of 42.37% after 100 cycles at 1 C. Even at a higher voltage range (2.7–4.5 V), where NCM811 can achieve a higher initial capacity of around 210 mA h g^{-1}, it still shows only modest capacity retention of 50% after 100 cycles.[32] In stark contrast, the Up-NCM-2 maintains 86.8% of its initial capacity after 100 cycles at 1 C, despite being cycled at an even higher upper cutoff voltage of 4.6 V, which typically accelerates degradation in nickel-rich cathodes. This superior cycling stability of Up-NCM-2 compared to NCM811 (86.8% *vs.* 50% retention)
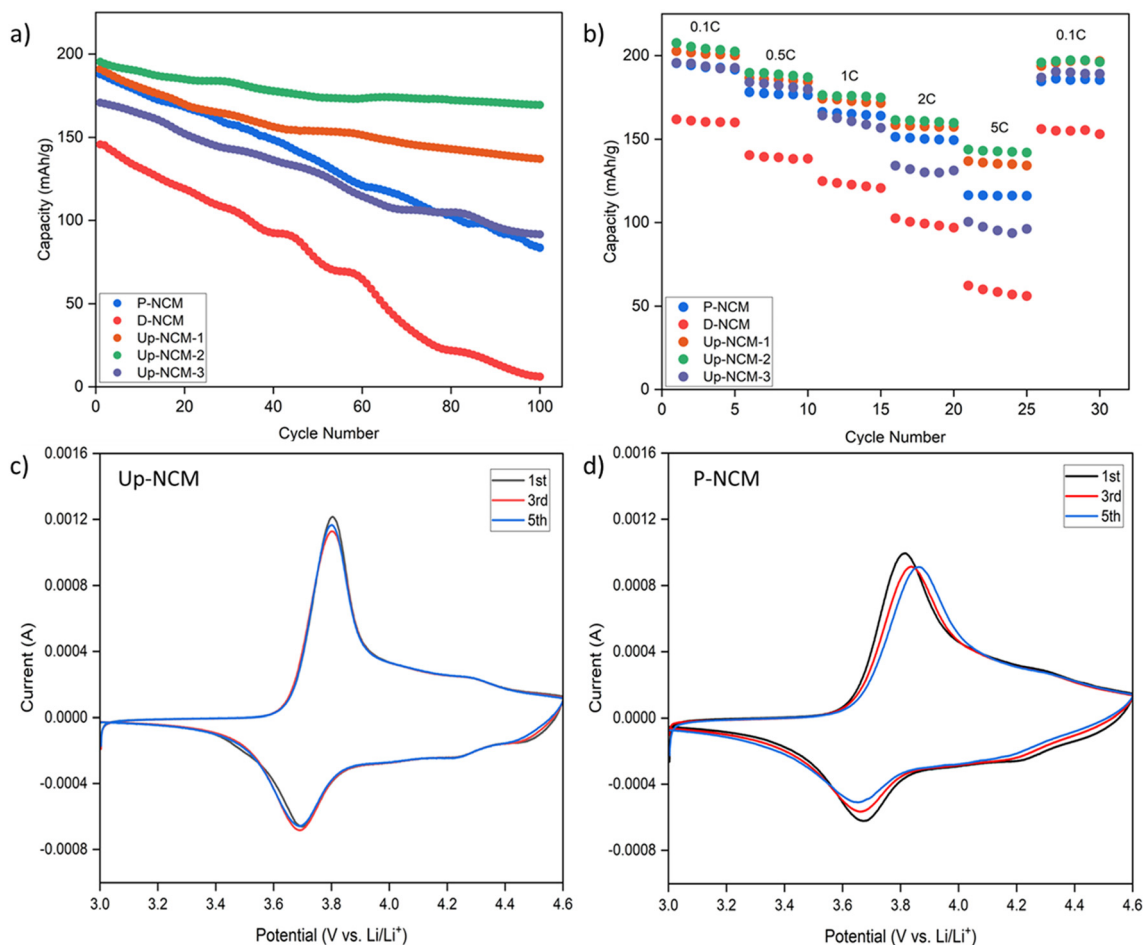
Fig. 4 Electrochemical performance of P-NCM, D-NCM, and Up-NCM with 1, 2, 3wt% LiAlO$_2$, (a) cycling performance, (b) rate capability, (c) CV curve of Up-NCM, (d) CV curve of P-NCM.

demonstrates the effectiveness of our upcycling strategy in balancing high capacity with exceptional long-term stability, which is crucial for practical battery applications.

To assess the impact of the LiAlO$_2$ coating layer on the rate capability, all samples were cycled under various current densities of 0.1, 0.5, 1, 2, and 5 C within a voltage range of 2.7–4.6 V. Fig. 4b illustrates the results, showing that P-NCM achieves a capacity of 116 mA h g^{-1} at 5 C, corresponding to a capacity retention of 59.4% relative to the capacity at 0.1 C. In comparison, the capacity of D-NCM at 5 C plummets to 56.1 mA h g^{-1} due to significant degradation. Remarkably, Up-NCM-2 demonstrates exceptional performance at all current densities, achieving a capacity of 141.9 mA h g^{-1} at 5 C with a capacity retention of 68.3%. This superior rate capability can be attributed to the low charge-transfer resistance and the fast Li$^+$ diffusion channels provided by the LiAlO$_2$ layer on the NCM particle surface. Up-NCM-1 with a lower amount of LiAlO$_2$, still surpasses P-NCM in rate capability with a capacity of 134.2 mA h g^{-1} at 5 C. Up-NCM-3 only delivers a capacity of 56 mA h g^{-1} at 5 C due to the sluggish electron transportation across the thick LiAlO$_2$ layer. Upon reverting to a lower current density of 0.1 C, the capacities of all samples are slightly lower than the

initial capacities at 0.1 C, which is a result of irreversible structural degradation induced by high current densities and high cut-off voltages. Comparing the Up-NCM-2 with reported NCM811 materials reveals a substantial advantage in rate performance. While NCM811 can only deliver a capacity of 103.61 mA h g^{-1} at 5 C, Up-NCM-2 achieves a significantly higher capacity of 141.9 mA h g^{-1} at the same rate, representing a 37% improvement. This enhanced rate capability of Up-NCM-2 can be attributed to the synergistic effects of the optimized LiAlO$_2$ coating, which creates efficient Li$^+$ diffusion pathways while maintaining adequate electronic conductivity. Despite having a lower nickel content than NCM811, the Up-NCM-2 demonstrates that proper surface engineering can effectively compensate for the theoretical capacity advantages of higher-nickel formulations, particularly at elevated current densities where electrode kinetics become the limiting factor.

To conduct a thorough evaluation of electrochemical performance, cyclic voltammetry (CV) analyses were performed on the samples within a voltage range of 2.7–4.6 V at a scan rate of 0.1 mV s^{-1}. The CV curves for P-NCM and Up-NCM are depicted in Fig. 4c and d, respectively. Each sample exhibited a pair of redox peaks, indicating the Ni^{2+}/Ni^{3+} oxidation/

reduction processes. Notably, the oxidation peaks of Up-NCM remain constant at 3.8 V across the 1st, 3rd, and 5th cycles, whereas the oxidation peaks of P-NCM, initially at 3.8 V during the first cycle, shifted to 3.86 V by the fifth cycle. This stability of oxidation peak positions in Up-NCM suggests a higher electrochemical reversibility compared to P-NCM. Further evidence of improved electrochemical properties is seen that the potential difference (ΔE) between the oxidation and reduction peaks was significantly lower in Up-NCM (0.102 V) than in P-NCM (0.22 V), indicating that the LiAlO$_2$ coating layer effectively reduces interface polarization within the NCM structure. This reduction in polarization is attributed to the protection provided by the LiAlO$_2$ coating layer against the formation of a non-conductive rock-salt layer on the NCM particle surface, a consequence of structural degradation at high cut-off voltages.[33] In addition to reaction reversibility and reduced polarization, the high oxidation peak intensity observed in Up-NCM shows enhanced kinetics of the electrochemical reactions compared to those in P-NCM, further highlighting the positive impact of the LiAlO$_2$ coating on the electrochemical performance of NCM.

To further understand the improvement of the LiAlO$_2$ coating layer in Li$^+$ diffusion, Electrochemical Impedance Spectroscopy (EIS) was employed to measure the impedance of the samples in their fully discharged state before and after three formation cycles. As illustrated in Fig. 5a and b, all samples displayed a semi-circle in the high-frequency range and a sloping line in the low-frequency range. The semi-circle is indicative of the combined resistance of the solid electrolyte interface (SEI) and charge transfer, while the sloping line is associated with the Warburg impedance, reflecting Li$^+$ diffusion through the electrode. Given that the formation conditions for all samples were identical, the SEI resistance (R_{sei}) is presumed constant across the samples, allowing the value of the semi-circle to primarily reflect charge-transfer resistance (R_{ct}). The equivalent circuit model used for EIS curve fitting is presented in Fig. 5d. Both P-NCM and Up-NCM samples exhibit comparable bulk resistance (R_b) both before and after the formation cycles. Before formation, all samples show significantly high impedance values primarily attributable to charge transfer resistance, with P-NCM exhibiting the highest R_{ct} of 787.4Ω due to its unprotected surface. Initially, the R_{ct} values for Up-NCM samples were significantly lower than those for P-NCM, attributable to the presence of the LiAlO$_2$ coating. Among them, Up-NCM-2, with its optimal LiAlO$_2$
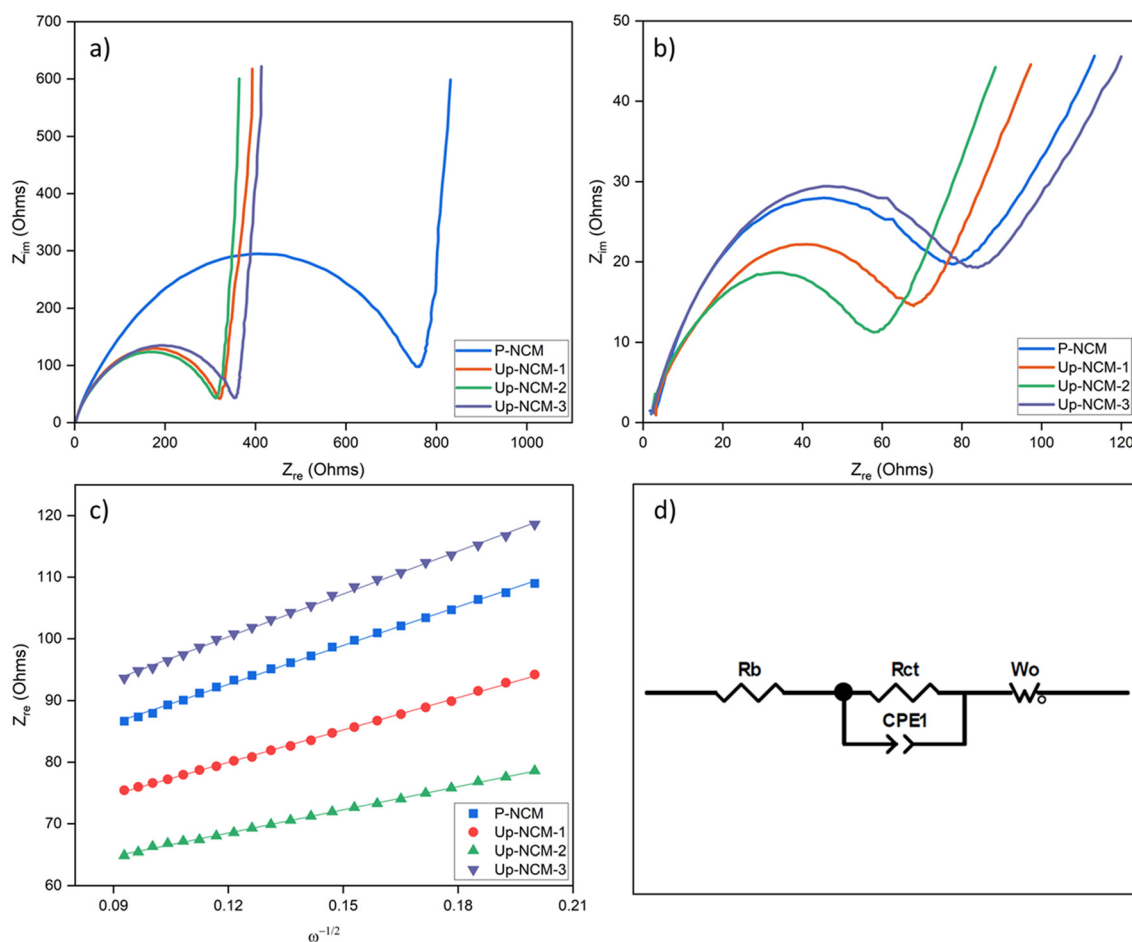

Fig. 5 EIS curve of P-NCM and Up-NCM with 1, 2, 3wt% LiAlO$_2$, (a) before formation, (b) after formation, (c) Relationship of Z' and $\omega^{-1/2}$, (d) Equivalent circuit for EIS fitting.

coating ratio, showed the lowest R_{ct} of 312.1 Ω. After formation cycles, a dramatic decrease in overall impedance is observed for all samples, indicating the successful formation of a stable SEI layer on the electrode surface. The R_{ct} values decrease by an order of magnitude, with Up-NCM-2 showing the lowest value of 57.9 Ω, compared to 70.4 Ω of P-NCM. This reduction in R_{ct} for Up-NCM-2 underscores the ability of the $LiAlO_2$ coating to facilitate rapid Li^+ diffusion. The Li^+ diffusion coefficient within the electrode bulk is directly correlated with the Warburg impedance, which is derived from the slope of the straight line in the $Z_{re} \sim \omega^{-1/2}$ plot. Thus, the Li^+ diffusion coefficient can be calculated based on the following equations:

$$D_{Li^+} = \frac{R^2 T^2}{2A^2 n^4 F^4 c^2 \sigma^2} \quad (4)$$

$$Z_{re} = R_b + R_{ct} + \sigma\omega^{-1/2} \quad (5)$$

where, R is the gas constant (8.31446 J mol^{-1} K^{-1}), T is absolute temperature (298.15 K), A is the surface area of the electrode (0.96987 cm^2, D = 1.11 cm), n is the electron number (1 for Li^+), F is the Faraday constant (96 485.33 C mol^{-1}), c is the lithium ion concentration (1 mol L^{-1}), and σ is the Warburg factor, which is the slope of the straight line in Fig. 5c.

Based on the equations, the Li^+ diffusion coefficient is shown in Table 1. Up-NCM-2 achieves the highest Li^+ diffusion coefficient (D_{Li^+}), which is 1.228×10^{-12} cm^2 S^{-1}. Even though Up-NCM-1 has a lower $LiAlO_2$ ratio than Up-NCM-2, it still exhibits an enhanced D_{Li^+} compared to 8.601×10^{-13} cm^2 S^{-1} of P-NCM. This enhancement in Li^+ diffusion for Up-NCM-1 and Up-NCM-2 relative to P-NCM illustrates the positive impact of the $LiAlO_2$ coating on lithium-ion transport. However, it is noted that the D_{Li^+} decreases with increasing weight ratio of the coating layer. This decline is attributed to the excessive thickness of the $LiAlO_2$ coating which impedes lithium-ion transport.

The thermal stability of the NCM cathode is of great importance, since it is directly related to the safety of lithium-ion batteries. To evaluate this critical property, the thermogravimetric analysis (TGA) was conducted to compare the thermal stability of P-NCM, D-NCM, and Up-NCM in the temperature range of 25–400 °C. As shown in Fig. 6, D-NCM exhibits a large weight loss starting from 150 °C, which is attributed to the decomposition of D-NCM due to the unstable structure of D-NCM caused by the lithium loss and structural degradation. Through the upcycling process, the D-NCM was regenerated
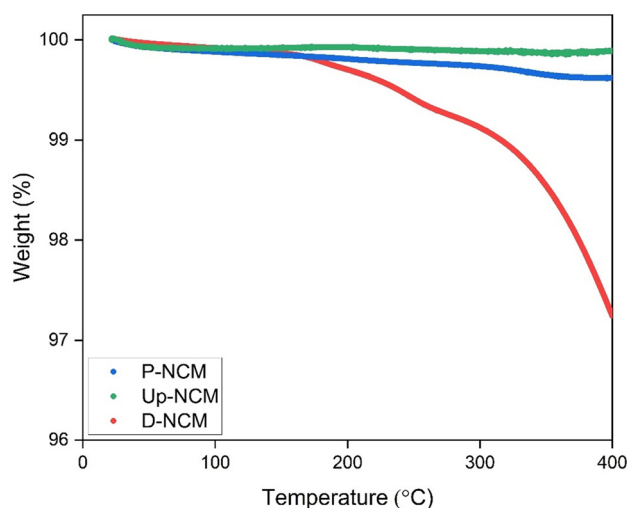

Fig. 6 TGA curve of P-NCM, D-NCM, and Up-NCM.

and was covered with a $LiAlO_2$ coating layer. As a result of the surface engineering, Up-NCM shows a significantly enhanced thermal stability with only 0.1% weight loss across the temperature range, which is better than the 0.4% of P-NCM. The results clearly prove that the thermal stability of degraded cathode materials is effectively recovered and improved by the proposed upcycling process.

Conclusion

Here we report the development of a novel two-step upcycling method that integrates a low-temperature annealing process with a $LiAlO_2$ coating process to regenerate degraded NCM622 with enhanced electrochemical performance. Through this upcycling process, the lithium deficiency and structural degradation of D-NCM are effectively recovered, resulting in upcycled NCM622 with a $LiAlO_2$ coating layer demonstrating high initial capacity, cycling stability, and rate capability. The $LiAlO_2$ coating layer plays a crucial role in reducing interface polarization and enhancing the electrochemical reversibility of NCM. Additionally, the low charge-transfer resistance and high Li^+ diffusion coefficient confirm the presence of fast Li^+ diffusion channels provided by the $LiAlO_2$ coating layer. Thermogravimetric analysis (TGA) results indicate that the upcycled NCM622 with a $LiAlO_2$ coating layer exhibits superior thermal stability compared to the pristine material. Based on the findings of this study, the upcycled NCM622 with a $LiAlO_2$ coating layer demonstrates superior electrochemical performance and thermal stability compared to the pristine counterpart. These improvements have significant practical implications, as this advancement enables the reuse of such cathode materials in new lithium-ion batteries with high performance requirements, thereby reducing costs, environmental impacts, and enhancing sustainability. In conclusion, the results of this study highlight the potential of upcycling

Table 1 EIS fitting results

Sample	Before formation		After formation		
	R_b (Ω)	R_{ct} (Ω)	R_b (Ω)	R_{ct} (Ω)	D_{Li^+} (cm^2 S^{-1})
P-NCM	1.957	787.4	2.112	70.4	8.601×10^{-13}
Up-NCM-1	2.024	329.9	1.925	65.6	1.228×10^{-12}
Up-NCM-2	2.017	312.1	1.910	57.9	2.358×10^{-12}
Up-NCM-3	1.912	360.4	1.970	78.4	7.019×10^{-13}

degraded NCM for high electrochemical performance, high safety, and low-cost lithium-ion battery.

Data availability

The data supporting this article have been included as part of the ESI.†

Conflicts of interest

There are no conflicts to declare.

Acknowledgements

References

1 M. Broussely and G. Archdale, Li-ion batteries and portable power source prospects for the next 5–10 years, *J. Power Sources*, 2004, **136**(2), 386–394.

2 W. Mrozik, M. A. Rajaeifar, O. Heidrich and P. Christensen, Environmental impacts, pollution sources and pathways of spent lithium-ion batteries, *Energy Environ. Sci.*, 2021, **14**(12), 6099–6121.

3 Y. Shi, M. Zhang, Y. S. Meng and Z. Chen, Ambient–pressure relithiation of degraded $Li_xNi_{0.5}Co_{0.2}Mn_{0.3}O_2$ (0 < x < 1) via eutectic solutions for direct regeneration of lithium–ion battery cathodes, *Adv. Energy Mater.*, 2019, **9**(20), 1900454.

4 P. Xu, Q. Dai, H. Gao, H. Liu, M. Zhang, M. Li, Y. Chen, K. An, Y. Meng, P. Liu, Y. Li, J. Spangenberger, L. Gaines, J. Lu and Z. Chen, Efficient direct recycling of lithium-ion battery cathodes by targeted healing, *Joule*, 2020, **4**(12), 2609–2626.

5 Y. Wang, H. Yu, Y. Liu, Y. Wang, Z. Chen, D. Tang, W. Li and J. Li, Sustainable regenerating of high-voltage performance $LiCoO_2$ from spent lithium-ion batteries by interface engineering, *Electrochim. Acta*, 2022, **407**, 139863.

6 Z. Qin, Y. Zhang, W. Luo, T. Zhang, T. Wang, L. Ni, H. Wang, N. Zhang, X. Liu, J. Zhou and G. Chen, A Universal Molten Salt Method for Direct Upcycling of Spent Ni–rich Cathode towards Single–crystalline Li–rich Cathode, *Angew. Chem., Int. Ed.*, 2023, **62**(25), e202218672.

7 K. S. Kim, M. K. Jeon, S. H. Song, S. Hong, H. S. Kim, S. W. Kim, J. Kim, P. Oh, J. Hwang, J. Song, J. J. Woo, S. H. Yu and H. Kim, Upcycling spent cathodes into single-crystalline Ni-rich cathode materials through selective lithium extraction, *J. Mater. Chem. A*, 2023, **11**(39), 21222–21230.

8 X. Ma, J. Hou, P. Vanaphuti, J. Fu, L. Azhari, Y. Liu and Y. Wang, Direct upcycling of mixed Ni-lean polycrystal to single-crystal Ni-rich cathode materials, *Chem*, 2022, **8**(7), 1944–1955.

9 C. Xing, H. Da, P. Yang, J. Huang, M. Gan, J. Zhou, Y. Li, H. Zhang, B. Ge and L. Fei, Aluminum Impurity from Current Collectors Reactivates Degraded NCM Cathode Materials toward Superior Electrochemical Performance, *ACS Nano*, 2023, **17**(3), 3194–3203.

10 H. Ji, J. Wang, H. Qu, J. Li, W. Ji, X. Qiu, Y. Zhu, H. Ren, R. Shi, G. Ji, W. Zhao and G. Zhou, Closed–Loop Direct Upcycling of Spent Ni–Rich Layered Cathodes into High–Voltage Cathode Materials, *Adv. Mater.*, 2024, **36**(36), 2407029.

11 T. Wang, H. Luo, J. Fan, B. P. Thapaliya, Y. Bai, I. Belharouak and S. Dai, Flux upcycling of spent NMC 111 to nickel-rich NMC cathodes in reciprocal ternary molten salts, *iScience*, 2022, **25**(2), 103801.

12 J. Shen, M. Zhou, W. Tang, Q. Huang, H. Pi, W. Liu, R. Liu and L. Li, Surface Reconstruction Strategy enables Rapid Upcycling Highly Degraded Layered Cathode, *Nano Energy*, 2025, **136**, 110741.

13 M. Jiang, D. L. Danilov, R. A. Eichel and P. H. Notten, A review of degradation mechanisms and recent achievements for Ni–rich cathode–based Li–ion batteries, *Adv. Energy Mater.*, 2021, **11**(48), 2103005.

14 L. Li, Z. Chen, Q. Zhang, M. Xu, X. Zhou, H. Zhu and K. Zhang, A hydrolysis-hydrothermal route for the synthesis of ultrathin $LiAlO_2$-inlaid $LiNi_{0.5}Co_{0.2}Mn_{0.3}O_2$ as a high-performance cathode material for lithium ion batteries, *J. Mater. Chem. A*, 2015, **3**(2), 894–904.

15 J. Luo, J. X. Liu, F. M. Xiao, L. Huang, W. C. Li, R. H. Tang, Q. Zhou and Y. Wang, Design of $LiAlO_2$ mosaic structure for preparing high nickel-based $LiNi_{0.88}Co_{0.07}Al_{0.05}O_2$ cathode material by simple hydrolysis method, *Electrochim. Acta*, 2021, **375**(10), 137974.

16 B. Huang, Z. Zhao, Y. Sun, M. Wang, L. Chen and Y. Gu, Lithium-ion conductor $LiAlO_2$ coated $LiNi_{0.8}Mn_{0.1}Co_{0.1}O_2$ as cathode material for lithium-ion batteries, *Solid State Ionics*, 2019, **338**, 31–38.

17 H. S. Kim, Y. Kim, S. I. Kim and S. W. Martin, Enhanced electrochemical properties of $LiNi_{1/3}Co_{1/3}Mn_{1/3}O_2$ cathode material by coating with $LiAlO_2$ nanoparticles, *J. Power Sources*, 2006, **161**(1), 623–627.

18 S. Dong, Y. Zhou, C. Hai, J. Zeng, Y. Sun, Y. Ma, Y. Shen, X. Li, X. Ren, C. Sun, G. Zhang and Z. Wu, Enhanced cathode performance: Mixed Al_2O_3 and $LiAlO_2$ coating of $Li_{1.2}Ni_{0.13}Co_{0.13}Mn_{0.54}O_2$, *ACS Appl. Mater. Interfaces*, 2020, **12**(34), 38153–38162.

19 W. Tang, Z. Chen, F. Xiong, F. Chen, C. Huang, Q. Gao, T. Wang, Z. Yang and W. Zhang, An effective etching-induced coating strategy to shield $LiNi_{0.8}Co_{0.1}Mn_{0.1}O_2$ electrode materials by $LiAlO_2$, *J. Power Sources*, 2019, **412**(1), 246–254.

20 J. Gao, S. Shi, R. Xiao and H. Li, Synthesis and ionic transport mechanisms of α-$LiAlO_2$, *Solid State Ionics*, 2016, **286**, 122–134.

21 C. Usubelli, M. M. Besli, S. Kuppan, N. Jiang, M. Metzger, A. Dinia, J. Christensen and Y. Gorlin, Understanding the

overlithiation properties of $LiNi_{0.6}Mn_{0.2}Co_{0.2}O_2$ using electrochemistry and depth-resolved X-ray absorption spectroscopy, *J. Electrochem. Soc.*, 2020, **167**(8), 080514.

22 D. Mohanty, S. Kalnaus, R. A. Meisner, K. J. Rhodes, J. Li, E. A. Payzant, D. L. Wood and C. Daniel, *J. Power Sources*, 2013, **229**, 239.

23 D. Mohanty and H. Gabrisch, Microstructural investigation of $Li_xNi_{1/3}Mn_{1/3}Co_{1/3}O_2$ ($x \leq 1$) and its aged products via magnetic and diffraction study, *J. Power Sources*, 2012, **220**, 405–412.

24 C. H. Jung, H. Shim, D. Eum and S. H. Hong, Challenges and recent progress in $LiNi_xCo_yMn_{1-x-y}O_2$ (NCM) cathodes for lithium ion batteries, *J. Korean Ceram. Soc.*, 2021, **58**(1), 1–27.

25 H. Zhang, F. Omenya, M. S. Whittingham, C. Wang and G. Zhou, Formation of an anti-core–shell structure in layered oxide cathodes for Li-ion batteries, *ACS Energy Lett.*, 2017, **2**(11), 2598–2606.

26 L. Lei, D. He, Y. Zou, W. Zhang, Z. Wang, M. Jiang and M. Du, Phase transitions of $LiAlO_2$ at high pressure and high temperature, *J. Solid State Chem.*, 2008, **181**(8), 1810–1815.

27 M. Shang and L. Peng, The regeneration and electrochemical performance study of NCM622 cathode materials, *Ionics*, 2021, **27**(2), 527–532.

28 R. S. Negi, Y. Yusim, R. Pan, S. Ahmed, K. Volz, R. Takata, F. Schmidt, A. Henss and M. T. Elm, A Dry–Processed

29 M. Guo, Y. Luo, L. Yan, T. Lv, Y. Gao, C. Shen, K. Xie and J. Xie, Degradation mechanism of $LiNi_{0.5}Co_{0.2}Mn_{0.3}O_2$/graphite cells at elevated state of charge and high temperature, *J. Electrochem. Soc.*, 2020, **167**, 160528.

30 W. Tang, Z. Chen, H. Huang, M. Irfan, C. Huang, Z. Yang and W. Zhang, PVP-bridged γ-$LiAlO_2$ nanolayer on $Li_{1.2}Ni_{0.182}Co_{0.08}Mn_{0.538}O_2$ cathode materials for improving the rate capability and cycling stability, *Chem. Eng. Sci.*, 2021, **229**, 116126.

31 Y. Hu, A. Ruud, V. Miikkulainen, T. Norby, O. Nilsen and H. Fjellvåg, Electrical characterization of amorphous LiAlO2 thin films deposited by atomic layer deposition, *RSC Adv.*, 2016, **6**(65), 60479–60486.

32 M. Zhang, M. Lv, D. Zhang, Y. Yan, Y. Wang, J. Li and Z. Li, Enhanced electrochemical properties of NCM811 cathode material due to synergistic modification with Sm as doping and coating agent, *J. Alloys Compd.*, 2022, **909**, 164712.

33 S. H. Song, M. Cho, I. Park, J. G. Yoo, K. T. Ko, J. Hong, J. Kim, S. K. Jung, M. Avdeev, S. Ji, S. Lee, J. Bang and H. Kim, High–voltage–driven surface structuring and electrochemical stabilization of Ni–rich layered cathode materials for Li rechargeable batteries, *Adv. Energy Mater.*, 2020, **10**(23), 2000521.

Al$_2$O$_3$/LiAlO$_2$ Coating for Stabilizing the Cathode/Electrolyte Interface in High–Ni NCM–Based All–Solid–State Batteries, *Adv. Mater. Interfaces*, 2022, **9**(8), 2101428.